

# On the Structural Shape Optimization through Variational Methods and Evolutionary Algorithms

Fernando Fraternali,<sup>1</sup> Andrea Marino,<sup>1</sup> Tamer El Sayed,<sup>2</sup>  
and Antonio Della Cioppa<sup>3</sup>

<sup>1</sup>Department of Civil Engineering, University of Salerno, Salerno, Italy

<sup>2</sup>Division of Engineering and Applied Science, California Institute of Technology, Pasadena, CA, USA

<sup>3</sup>Department of Information and Electrical Engineering, University of Salerno, Italy

---

We employ the variational theory of optimal control problems and evolutionary algorithms to investigate the form finding of minimum compliance elastic structures. Mathematical properties of ground structure approaches are discussed with reference to arbitrary collections of structural elements. A numerical procedure based on a Breeder Genetic Algorithm is proposed for the shape optimization of discrete structural models. Several numerical applications are presented, showing the ability of the adopted search strategy in avoiding local optimal solutions. The proposed approach is validated against a parade of results available in the literature.

---

**Keywords** shape optimization, optimal control, ground structures, compliance optimization, evolutionary algorithms.

## 1. INTRODUCTION

The formulation of mathematical methods to achieve an optimal structural design, according to static, functional and/or aesthetic criteria, has constantly attracted the attention of engineers and architects. Graphical constructions, reduced scale models and physical analogies have been used in the past (see, e.g., [1–3]) to assist in the creative phase of the design process [4, 5]. Mirabile anticipations of modern tools of conceptual design are found in the work of the Spanish architect A. Gaudí on funicular structures, organic shapes and curved surfaces. They can also be found in the studies of J. C. Maxwell on fully-stressed trusses and the research of A. G. M. Michell on optimal arrays of orthogonal trusses (cf. e.g.) [2, 6, 7].

In the most recent literature, shape (or geometry) optimization is identified with the particular stage of *structural optimization*, which deals with the search of the optimal configuration of a design domain. It is usually performed by moving the boundaries of an initial trial configuration in order to min-

imize (or maximize) an objective function under suitable design constraints. Structural optimization involves optimal cross-sectional dimensions (*sizing optimization*) and optimal connectivity of structural components (*topology optimization*). In some cases, the term generalized shape optimization, or topology optimization, is used to indicate the entire structural optimization process. Typical optimization objectives are minimal weight, minimal compliance (or maximal stiffness), optimal eigenfrequencies, and maximal structural ductility. Optimal design constraints often include material volume, displacement, stiffness, stress and buckling loads.

Both discrete and continuous approaches to structural optimization have been formulated over the past 50 years. Discrete models are formed by constructing finite collections of structural elements, whose positions, dimensions and connectivity are subject to optimization. In these collections, elements can be removed to establish a *ground structure*. This particular approach was introduced in the 1960's for truss structures [8] and is still rather active (see, e.g., [9–16]). On the other hand, continuous models consist of one or multiple design domains made up of composite materials with perforated periodic microstructures. The optimal material distribution is found by optimizing the design variables associated with the microstructures and making use of the *homogenization theory*. This approach was introduced at the end of the 1980s [17] and has been applied to a wide range of technical problems (cf. [18–27]).

As for optimization algorithms, *mathematical programming methods* were largely used during the 1960s for ground structure problems. In more recent years, the necessity of solving problems with a large number of design variables has led researchers to formulate more powerful optimization algorithms, such as *optimality criteria* ([17, 28, 29]), *sequential approximate optimization* methods ([30–33]), and *evolutionary structural optimization* ([34–36]). These methods are *gradient based* and make use of sensitivity analysis. Methods which are not based on gradients (*gradient less* or *heuristic methods*), such as *simulated annealing* ([37, 38]), *genetic algorithms* ([39–43]), *evolutionary computation* ([44–48]), and *biological*

---

Received 29 February 2008; accepted 26 July 2008  
Address correspondence to Fernando Fraternali, Department of Civil Engineering, University of Salerno, 84084, Fisciano, Italy.  
E-mail: f.fraternali@unisa.it

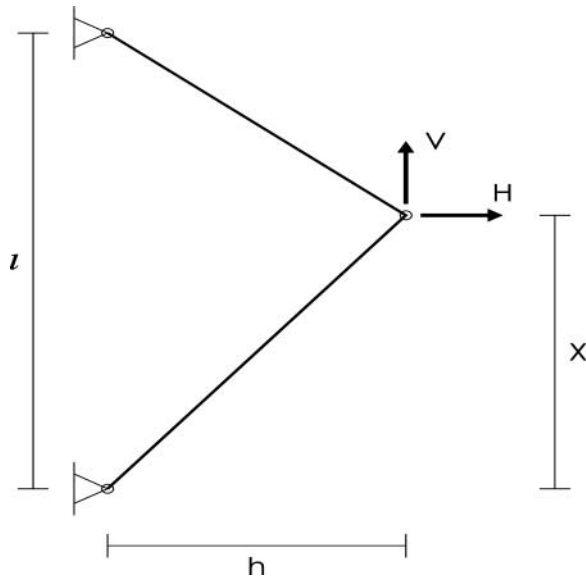


FIG. 1. Truss structure with an adoptive node.

*growth* ([49–51]), have also been introduced. In comparison to gradient methods, heuristic approaches may require longer computational times, however, they do not require elaborate knowledge of the search environment, can provide multiple sub-optimal solutions, and are capable of handling a wide range of technical problems. Moreover, heuristic methods take advantage of computational parallelization, which can overcome the hurdle of longer computational times.

Generalized shape optimization problems are not often well posed, i.e., affected by lack of existence of solutions unless suitable *relaxations* are introduced [52]. This is usually the case when continuous formulations are employed and the competing objects are domains instead of functions or scalar parameters ([53]). On the other hand, when existence is established, such problems are typically *non convex* and characterized by multiple local optima.

An elementary benchmark example is offered by the minimum compliance problem of the ground structure shown in Figure 1. One can take the vertical coordinate  $X$  of the loaded node as the unique design variable and set all the remaining geometrical and mechanical quantities involved ( $h, l, H, V$ ; extensional stiffness of the bars) to 1, in consistent units. In the linear elastic regime, the *strain energy*  $U$  can be computed at equilibrium as a function of  $X$  in order to obtain the two-well graph shown in Figure 2. This graph clearly illustrates that the examined problem is non convex, and that gradient based algorithms can easily get trapped at the local minima  $a$  in Figure 2. The local min-max compliance configurations of the structure are depicted in Figure 3.

This article deals with a numerical study on ground-structure approaches to shape optimization problems, which are modeled as *optimal control problems*. According to Bucur and Buttazzo [53], the existence of solutions is discussed in general form, regardless of the specific nature of the ground structure,

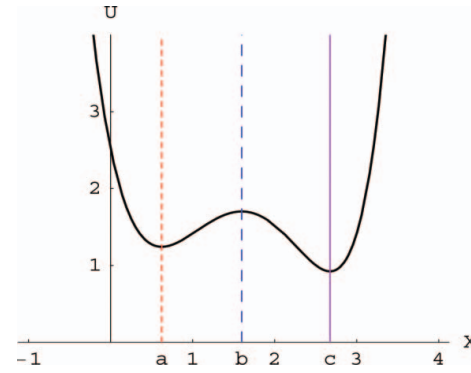


FIG. 2. Strain energy at equilibrium vs vertical position of the loaded node for the structure of Figure 1. (color figure provided online)

which can be composed of an arbitrary collection of truss, beam, plate, shell, and 3D elements. Attention is focused on linear elasticity and unconstrained minimization. The search for global optimal solutions is performed via evolutionary strategies, which naturally conform to the generality of the present approach. The peculiar features of these strategies and their ability in dealing with structural design optimization challenges, are well emphasized in [46]. It is also important to note their ability to avoid local optima and explore a search space of high dimensionality. They also demonstrate robustness and flexibility in the process of creative design. Genetic and evolutionary algorithms have been widely used in recent years for the optimal design of trusses and steel structures (cf. [46, 54] and references therein), and also in the design of airfoil structures [55]. Nevertheless, the potential of GAs and EAs for the structural design of more general structures and the automation of architectural design techniques still needs to be fully explored.

The present paper aims to pursue the following objectives:

- application of evolutionary strategies to the shape optimization of architectural and structural shapes made up of arbitrary assemblies of 1D, 2D, and/or 3D elements;

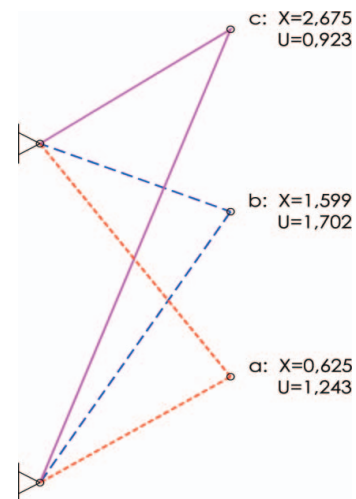


FIG. 3. Local min-max compliance configurations of the structure of Figure 1 (cf. Figure 2). (color figure provided online)

- numerical implementation of classical tools of shaping structures, such as graphical constructions of funicular curves and optimal thrust surfaces, requiring that the lines of thrust lie within a given design domain [1, 2, 3];
- computer simulation of the first stages of conceptual design dealing with simple bounds on design variables;
- execution of local/global optimization via suitable definitions of variable bounds.

We examine a parade of structural optimization examples, which involve the optimal shape of trusses, hanging cables and domes. The first example of Section. 4.1. shows the agility of the adopted Breeder Genetic Algorithm in handling a two-well non-convex problem. The examples of Sections. 4.2., 4.3. and 4.4. prove that funicular arches and optimal shapes of roofs can be conveniently obtained as minimum compliance shapes. All of the examined problems deal with global shape optimization, with the exception to those presented in Section. 4.3., which examine local optimization of spherical, baroque and gothic roof models. A specific example is dedicated to study the optimal shape of St. Peter's cupola in Rome. Here we establish a parallel with the conclusions of a renowned treatise by Giovanni Poleni [56] and known results about the statics of the cupola [57]. Relevant extensions and generalizations of the current study are discussed in the closing section.

## 2. A VARIATIONAL APPROACH TO SHAPE OPTIMIZATION

Let us consider the optimal shape problem of an open subset  $A$  of a design domain  $D$ , representing the reference configuration of an elastic body. The optimal shape minimizes a cost functional  $J(A, y)$ , where  $y$  denotes either the deformation mapping or the displacement field carrying  $A$  into the deformed configuration  $B$ .

Following Bucur and Buttazzo [53], we identify  $A$  with a control variable and  $y$  with a state variable, with the latter subject to the equilibrium equations of the body (state equations). We thus deal with an optimal control problem ruled by the following variational formulation

$$\min\{J(A, y) : A \in X, y \in \operatorname{argmin}G(A, \cdot) \subset Y\} \quad (1)$$

where now  $X$  is the set of controls,  $Y$  is the space of states, and  $G$  is the state functional given by

$$G(A, y) = \Pi(y) + \chi_{H(A)}(y) \quad (2)$$

with

$$\Pi(y) = \int_D (W(\nabla y) - \mathbf{b} \cdot y) dx \quad (3)$$

$$\chi_{H(A)}(y) = \begin{cases} 0 & \text{if } y \in H(A), \\ +\infty & \text{otherwise.} \end{cases} \quad (4)$$

In Eq. (2)–(4),  $W$  is the strain-energy density and  $\Pi$  is the total potential energy of the body. Furthermore, in the same equations,  $\mathbf{b}$  is the referential body force density per unit volume, and  $H(A)$  is the space of kinematically admissible deformations/displacements. The set of controls  $X$  coincides with the family of all open subsets of  $D$ . For the sake of simplicity, we assume that no surface forces are applied on the Neumann portion of  $\partial A$ , and that no optimization constraints are imposed.

A special case is that of minimum compliance problems of linear elastic bodies, where  $y$  is the displacement field and  $W$  is a quadratic function of  $\epsilon(y) := 1/2(\nabla y + \nabla y^T)$ . We let  $J$  coincide with the strain energy  $U$  of the body at equilibrium as follows

$$J = U(y_A) = \int_D W(\epsilon(y_A)) dx = \frac{1}{2} \int_D \mathbf{b} \cdot y_A dx \quad (5)$$

Here,  $y_A \in \operatorname{argmin} G(A, y)$ , and the Euler-Lagrange equations of the state functional (2.2) (principle of virtual work) have been employed. We note that, in this case,  $J$  does not depend explicitly on the control variable  $A$ .

We now introduce an adaptive triangulation  $T_h$  of  $A$ , and let  $\mathcal{T}_h$  indicate the set of topological and interpolation information encoded in  $T_h$ . Furthermore, we denote  $\mathbf{X}_h \in X_h \subset \mathfrak{R}^N$  and  $y_h \in Y_h \subset \mathfrak{R}^M$  to be the arrays collecting the Cartesian coordinates of the triangulation vertices (mesh nodes) in the reference and deformed configurations, respectively. We refer to  $N$  as the number of controls and to  $\mathbf{X}$  as the vector of controls. Finally, we introduce a family of finite element approximations  $\hat{y}_h(\mathcal{T}_h, \mathbf{X}_h, y_h)$  of  $y$  over  $T_h$ . A discrete formulation of Eq. (1) is as follows

$$\min \{ J_h(\mathcal{T}_h, \mathbf{X}_h, y_h) : \mathcal{T}_h \in \mathcal{M}_h, \mathbf{X}_h \in X_h, y_h \in \operatorname{argmin} G_h(\mathcal{T}_h, \mathbf{X}_h, \cdot) \subset Y_h \} \quad (6)$$

where

$$J_h(\mathcal{T}_h, \mathbf{X}_h, y_h) = J(\hat{y}_h(\mathcal{T}_h, \mathbf{X}_h, y_h)) \quad (7)$$

$$G_h(\mathcal{T}_h, \mathbf{X}_h, y_h) = G(\mathcal{T}_h, \mathbf{X}_h, \hat{y}_h(\mathcal{T}_h, \mathbf{X}_h, y_h)) \quad (8)$$

In Eq. (6),  $\mathcal{M}_h$  is a family of finite element meshes, generated, e.g., through recursive edge-swaps and local topological improvements of the given mesh  $T_h$  [58], [59].

Problem (6) applies to the topology and shape optimization of arbitrary ground structures, formed by any combinations of 1D, 2D and/or 3D elastic bodies/structures.

For fixed  $\mathcal{T}_h$  (geometry optimization), it is easy to prove that a solution always exists. One can observe that  $X_h$  is bounded since every node lies in  $\bar{D}$ . We will assume that  $X_h$  is a general compact subset of  $\mathfrak{R}^N$  to account for possible additional constraints which appear, e.g., if only a subset of nodes is allowed to move or if the nodes are only allowed to move in certain directions in the reference configuration. Taking into consideration that both the mappings  $\mathbf{X}_h \mapsto y_h \in \operatorname{argmin} G_h(\mathbf{X}_h, \cdot)$

and  $(X_h, y_h) \mapsto J_h(X_h, y_h)$  are continuous, the existence of the minimum of  $X_h \mapsto J_h(X_h, y_h(X_h))$  over the compact set  $X_h$  immediately follows from Weirstrass's extreme value theorem (see, e.g., [60]). Non-uniqueness has been shown in the previous paragraph by way of example.

Generalization of problem (6) to finite elasticity is straightforward through suitable modification of the cost function and the state functional (see, e.g., [58, 59]). Extensions to dissipative problems and dynamics can also be carried out through minimization of incremental energy functionals ([61–65]).

The next section illustrates the use of Evolutionary Algorithms for the search of the global minimum of  $J_h(X_h) := J_h(X_h, y_h(X_h))$ , considering simple shape optimization, minimum compliance problems and linearly elastic structures. The proposed search technique simply requires the iterative computation of the state variables and the cost (or fitness) function, and can be easily generalized to nonlinear and/or dynamical evolution problems (cf., e.g., [66]).

### 3. SHAPE OPTIMIZATION VIA EVOLUTIONARY ALGORITHMS

#### 3.1. Generality of Evolutionary Algorithms

The term Evolutionary Algorithms (EAs) refers to a family of probabilistic search methods inspired by the principle of Natural Evolution. In particular, EAs are based on concepts taken from Darwinian evolution of species, natural selection, and genetics. They are well suited for problems where the solution space is large and complex, i.e., multi-modal, discontinuous, and noisy [67].

These algorithms work on a population of individuals whose genotypes encode the features to be estimated. A genotype can be thought of as a set of genes, each one encoding one of the individual's features. To bootstrap the algorithm, a population of individuals is randomly generated and an iterative process, made up of two steps, is then entered. In the first step, the fitness of each individual is evaluated by measuring its performance by solving the problem at hand. In other words, each element of the population is evaluated in terms of a quantitative fitness, which represents the discriminant feature between a better phenotype and a worse one. This feature is defined by the probability that the organism will have to reproduce or as a function of the number of the offspring the organism has. In the second step, a new population is generated in the following way: pairs of individuals belonging to the current population are selected according to their fitness and mated by means of a recombination operator in order to generate new individuals. Such individuals are successively mutated with a set probability. The whole process is iterated until some termination criteria are fulfilled or a maximum number  $g$  of generations is reached.

#### 3.2. Breeder Genetic Algorithms

Breeder Genetic Algorithms (BGAs) [44, 47, 48] are more effective than other algorithms because they directly work with the variables to be optimized. Furthermore, selection mechanisms and genetic operators (mutation and recombination) are suited for a better and more efficient exploration of extremely large search spaces. In fact, in contrast to other EAs in which the selection is stochastic and meant to mimic Darwinian evolution, the BGA selection scheme is a deterministic one in which the fittest individuals are selected and entered into the gene pool to be recombined and mutated to form the new generation. By doing so, the best individuals are treated as super-individuals and mated together in order to create a fitter population. In the following sections, we discuss the selection mechanism, as well as the different types of genetic operators of BGAs; further details on these aspects can be found in [44, 47, 48].

#### 3.3. Individuals and Fitness

When applying BGAs (or EAs) to the shape optimization problems described in section. 2. it is natural to identify the individuals by the control vectors  $X_h \in X_h \subset \mathbb{R}^N$ , their genes with the single control variables (nodal coordinates)  $X_{h_1}, \dots, X_{h_N}$ , and their fitness with  $J_h(X_h, y_h(X_h))$ . The algorithm will sort the individuals in order of increasing fitness values such that the best individual (#1 on the list) will coincide with the minimum compliance “individual” of the given population.

For the sake of simplicity, we will hereafter drop the subscript  $h$  and employ the simplified notations  $X$  and  $J$  (or  $U$ ) for the search set  $X_h$  and the fitness  $J_h$ , respectively. The symbol  $X_i^t$  (or  $Y_i^t$ ,  $Z_i^t$ , etc.) will be instead used to denote the  $i$ th individual (control vector) of the generation number  $t$ , while the entire population at generation (or *time*)  $t$  will be denoted  $P^t$ .

#### 3.4. Selection

With regard to the selection mechanism, BGAs adopt the “Truncation” selection scheme where individuals are sorted according to their fitness and only the best individuals are selected to mate. The  $\mu$  best individuals are picked within the current population of  $\lambda$  elements as parents.  $T = \mu/\lambda$  is called the truncation threshold and indicates the proportion of the population selected to mate, while individuals below the truncation threshold do not produce offspring. Typical values of  $T$  are within the range 0.02 to 0.2. By doing so, the best individuals are treated as super-individuals and mated together, hoping that this will lead to a fitter population. As discussed previously, these concepts are taken from other sciences and mimic animal breeding. It should be noted that, when generating a new population, the best individual within the old population will always be retained in the next one, while the remaining  $\lambda - 1$  individuals are generated by selecting, mating and mutating individuals of the old population. The distribution of the selection probability  $p_s$  for

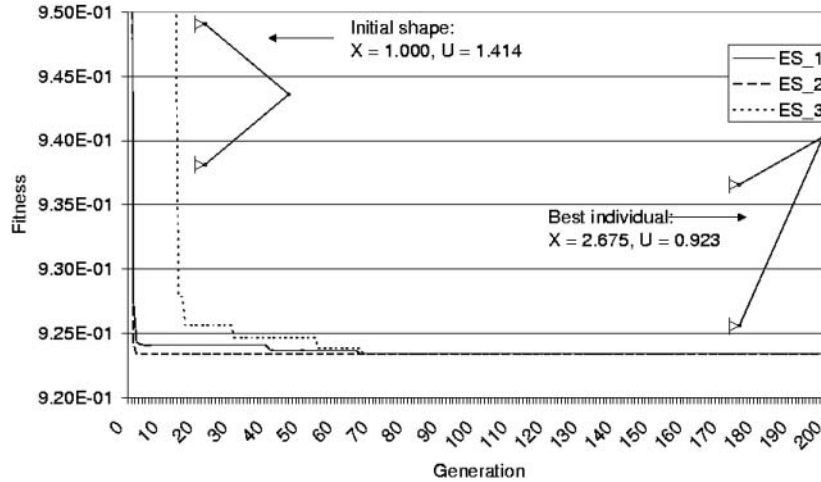


FIG. 4. BGA optimization of the truss structure in Figure 1. The horizontal axis shows the generation number and the vertical axis shows the corresponding best fitness (color figure provided online).

the truncation mechanism is given by the following mapping:

$$S : X_i^t \in P^t \rightarrow p_s(X_i^t) = \begin{cases} \frac{1}{\mu} & 1 \leq i \leq \mu \\ 0 & \mu < i \leq \lambda \end{cases} \quad (9)$$

### 3.5. Recombination and Mutation

In order to better define the genetic operators, let  $\mathbf{X} = (X_1, \dots, X_N)$  and  $\mathbf{Y} = (Y_1, \dots, Y_N)$  be two parents where  $X_i$  and  $Y_i$  are real variables. A recombination mechanism generates offspring from two parents; BGAs make use of three different recombination operators:

2. *Extended intermediate Recombination (EIR)*
3. *Extended Line Recombination (ELR)*

The discrete recombination generates corners of the hypercube defined by the parents, which is equivalent to exchanging values among individuals. According to this recombination scheme, each offspring will have the generic component  $Z_i$  given by  $X_i$  or  $Y_i$ , with a probability of 0.5 for each of them. In other words, if  $H(\mathbf{X}, \mathbf{Y})$  is the smallest hypercube containing  $\mathbf{X}$  and  $\mathbf{Y}$ , then  $\mathbf{Z}$  can only be a corner of  $H(\mathbf{X}, \mathbf{Y})$ . Denoting  $R$  as the recombination operator, one gets the following:

1. *Discrete recombination (DR)*

$$R_{dr} : (\mathbf{X}^t, \mathbf{Y}^t, p) \in X \times X \times [0, 1] \rightarrow \mathbf{Z}^{t+1} \in X \quad (10)$$

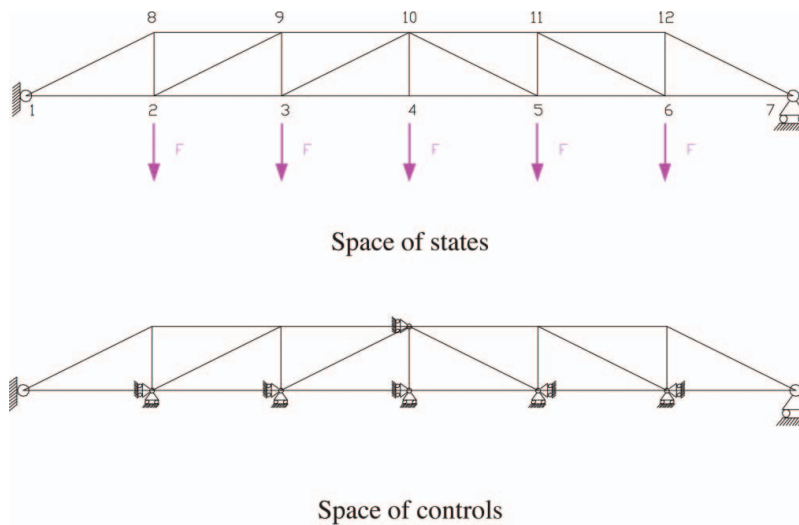


FIG. 5. Physical and design constraints for the optimal design of a truss structure (color figure provided online).

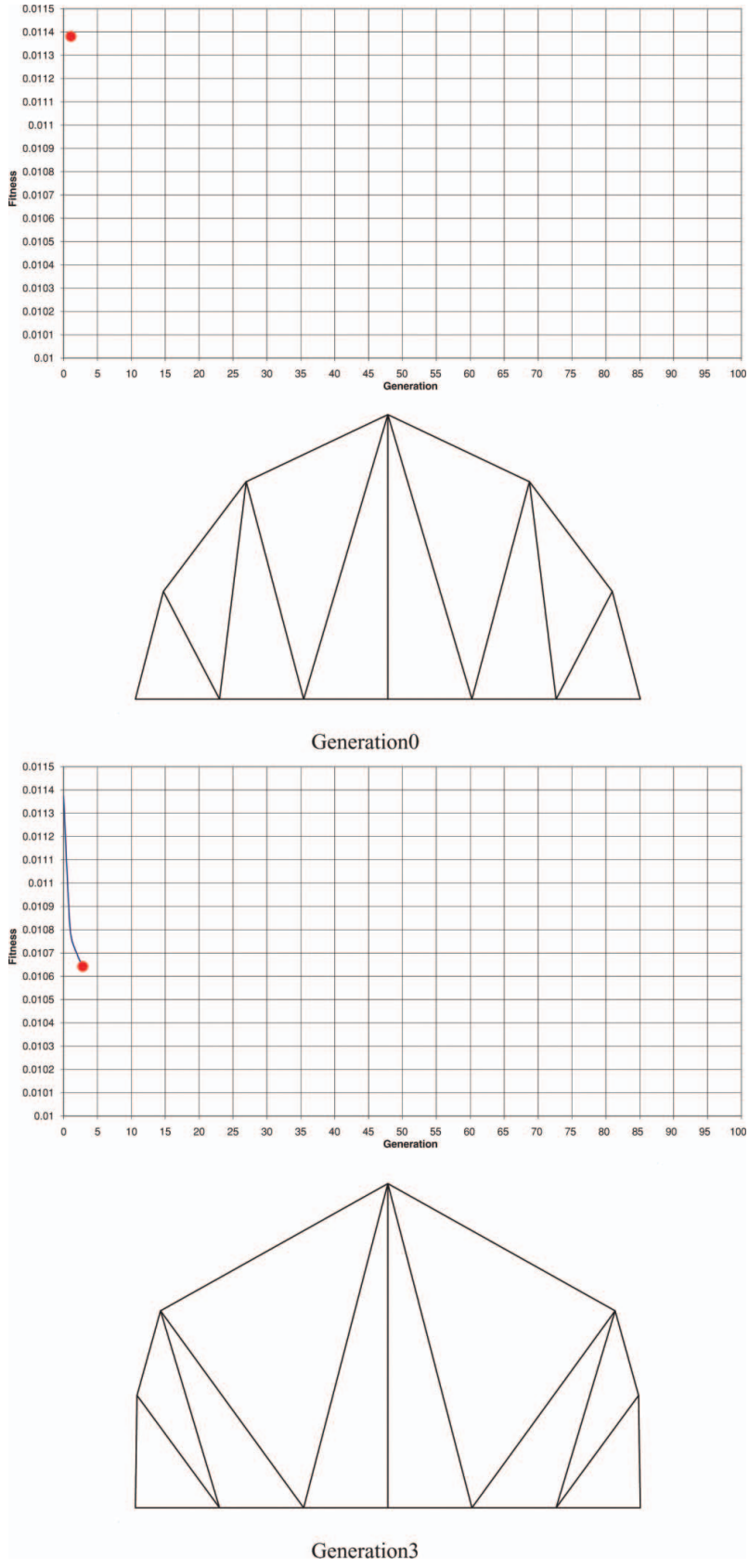
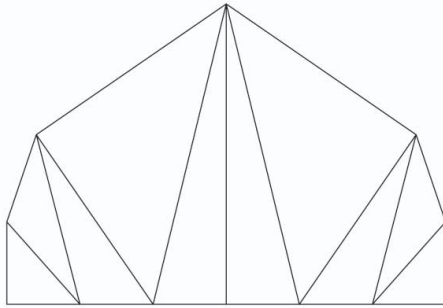
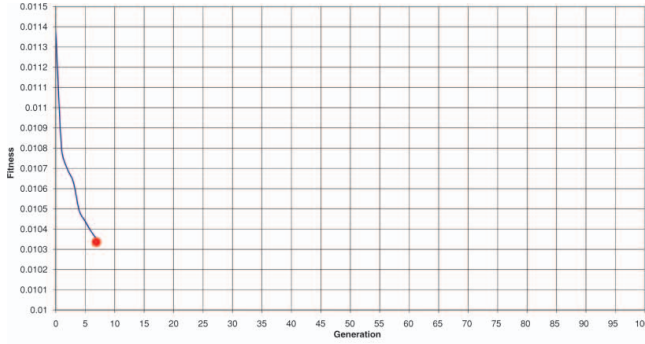
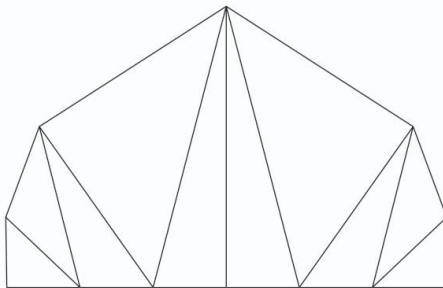
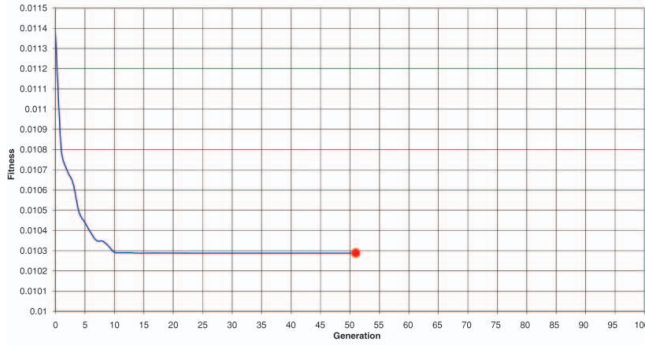


FIG. 6. BGA optimization of the truss in Figure 5. The horizontal axis shows the generation number and the vertical axis shows the corresponding normalized best fitness  $J/F L$ . The best shapes are shown below the corresponding plots.



Generation 7



Generation 51

FIG. 7. BGA optimization of the truss in Figure 5. The horizontal axis shows the generation number and the vertical axis shows the corresponding normalized best fitness  $J/FL$ . The best shapes are shown below the corresponding plots.

with

$$\mathbf{Z}^{t+1} = \begin{cases} \mathbf{X}^t, & p > 0.5 \\ \mathbf{Y}^t, & p \leq 0.5 \end{cases} \quad (11)$$

As for the Extended Intermediate Recombination, one should have the following:

$$R_{eir} : (\mathbf{X}^t, \mathbf{Y}^t, \mathbf{c}) \in X \times X \times [-d, 1 + d]^N \rightarrow \mathbf{Z}^{t+1} \in X \quad (12)$$

with

$$\mathbf{Z}_i^{t+1} = X_i^t + c_i (Y_i^t - X_i^t), \forall i \in \{1, \dots, N\} \quad (13)$$

where  $c_i$  is a scaling factor chosen uniformly at random over an interval  $[-d, 1 + d]$ , with  $d$  typically ranging in the interval  $[0, 0.5]$ . A good choice for  $d$  is 0.25, which allows the attainment of all the values belonging to the continuous interval between  $x_i$  and  $y_i$  and also allows for values outside the given interval. The Extended Line Recombination is similar to EIR, except for the choice of a unique scaling factor for all the variables:

$$R_{elr} : (\mathbf{X}^t, \mathbf{Y}^t, \mathbf{c}) \in X \times X \times [-d, 1 + d] \rightarrow \mathbf{Z}^{t+1} \in X \quad (14)$$

with

$$\mathbf{Z}_i^{t+1} = X_i^t + c (Y_i^t - X_i^t), \forall i \in \{1, \dots, N\} \quad (15)$$

where  $c$  is the global scaling factor. The difference between the two latter operators is that in the EIR a new  $c_i$  is to be evaluated for each component of the genotype vector, while in the ELR only one  $c$  is to be computed and used for all the components. As a consequence, EIR is capable of producing any point within a hypercube slightly larger than the one defined by the parents, while ELR can generate any point on the line defined by the parents in the search space. Mutation operators are very important because they are able to modify the speed of convergence and the dimension of the search space, and they have to be conveniently tuned to avoid a too fast and premature convergence, with the possibility to be trapped in local minima. As a consequence, the offspring are sometimes subject to mutation, in which single alleles are changed from parent to offspring.

Offspring variables are mutated by the addition of small random values (size of mutation step), with low probability. The probability of mutating a variable is set to be inversely proportional to the number of parameters to optimize. A mutation rate of  $1/N$  produces good results for a broad class of test functions. However, it has to be underlined that the mutation rate is independent of the population size and a self adaption of mutation rate during the evolution could be useful in some situations dealing with multi-modal functions. The mutation operator  $M : P^t \rightarrow P^{t+1}$  acts to randomly modify each vector  $\mathbf{X}^t$  by adding a random vector  $\mathbf{Y} = (Y_1, \dots, Y_N)$ , where each  $Y_i$  is scaled according to the search interval of  $X_i$ :

$$\mathbf{Z}^{t+1} = \mathbf{X}^t + \mathbf{Y} \quad (16)$$

The entries in  $\mathbf{Y}$  are normally distributed according to  $\mathcal{N}(0; \sigma)$  (Gaussian mutation) or  $\mathcal{U}(-\sigma; \sigma)$  (Uniform mutation), where  $\sigma$

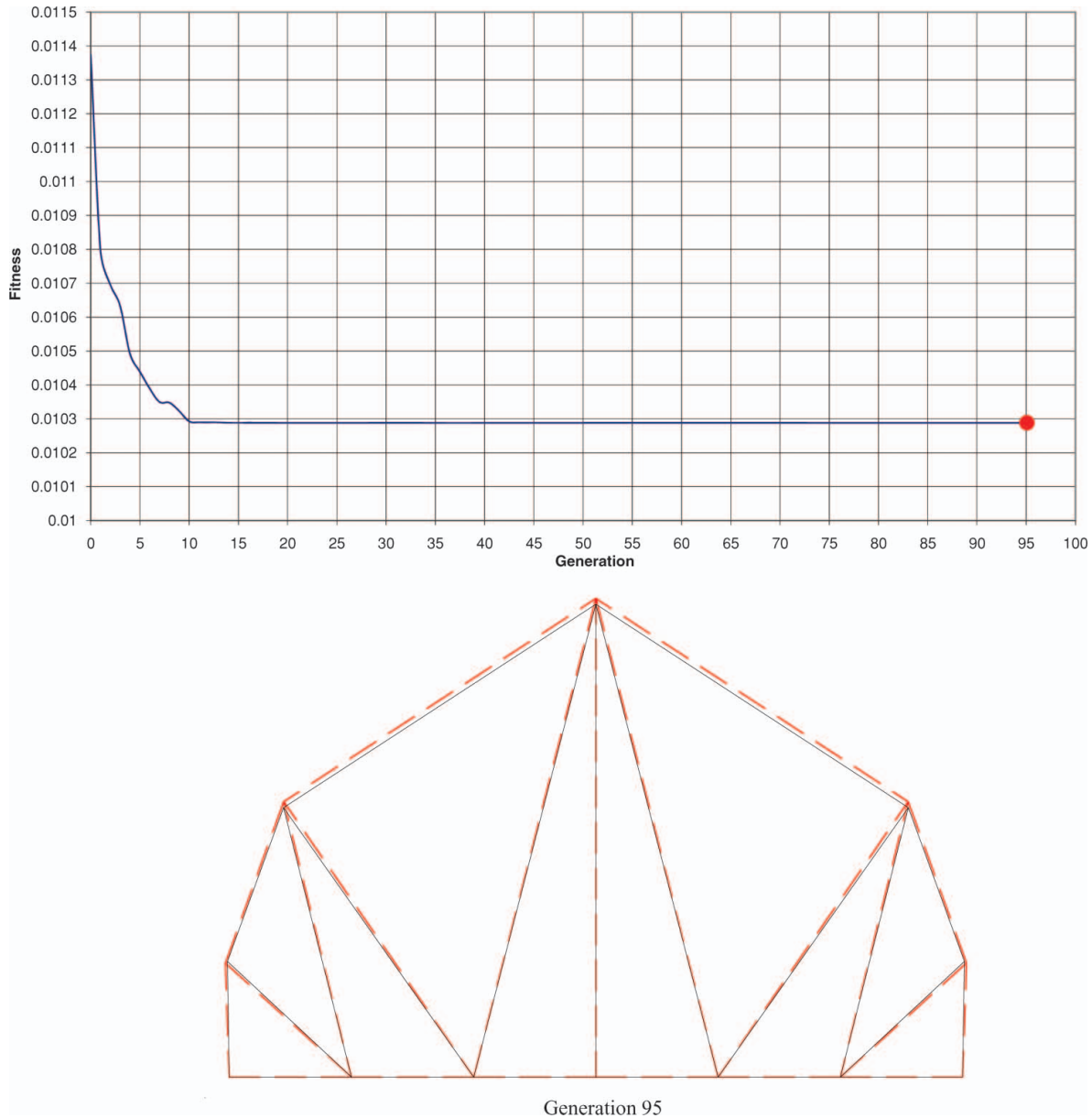


FIG. 8. Final best shape of the truss in Figure 5 obtained through the BGA optimization (solid line) in comparison with the optimal shape found by Brain in [70] (dashed line). The horizontal axis shows the generation number and the vertical axis shows the corresponding normalized best fitness  $J/FL$  (color figure provided online).

is defined as  $a \cdot (X_{i_{max}} - X_{i_{min}})$  and  $a$  is a scaling factor typically chosen in the range  $[0.01, 0.2]$ .

It should be noted that when a genetic operator generates a value for a parameter out of the range, the value is reported within the range by mirroring, i.e., by adding/subtracting the value of the limit of the range closest to it.

#### 4. NUMERICAL EXAMPLES

In the present section, we examine ground structures composed of linearly elastic beam and/or shell elements in order

to study the shape optimization of trusses and shell-like roof structures under different loading conditions. A specific example is dedicated to study the optimal shape of St. Peter's cupola in Rome, designed over the years by a collection of notable architects, including Donato Bramante, Michelangelo Buonarroti, and Antonio da Sangallo. The construction of St. Peter's basilica (*"La Macchina di San Pietro"* or *St. Peter's Machine*) began in 1506 and was only completed in 1626. The study of the cupola is carried out resuming the results of a famous treatise by Giovanni Poleni dated to 1748 [56], which was commissioned by Pope Benedict XV in 1743 to help restore the statics of that

marvelous structure having been affected at that age by diffuse fracture damage. It is interesting to note that the BGA minimum compliance shape of the cupola qualitatively corresponds to that indicated as optimal by Poleni in his treatise.

Preliminary sets of experiments were performed in order to select the most suitable genetic operators and to find the best values for their parameters. Based on these preliminary results, a tournament selection mechanism with a truncation threshold  $T$  of 0.2, EIR with  $d = 0.25$ , and Gaussian mutation with  $a = 0.1$ , were chosen. Moreover, the mutation rate was set to  $1/N$ , where  $N$  is the number of controls. In other words, one variable, on average, would be mutated for each individual. Finally, a total number of 150, 000 evaluations were allowed for each run. In each example, the elastic equilibrium problem of a given finite element model was solved using the commercial software SAP2000<sup>©</sup> [68], in correspondence with the current control vector or “individual”  $X$ .

#### 4.1. Truss Structures

The strain energy of a linearly elastic truss structure can be written as (refer, e.g., to Washizu [69])

$$J(\mathbf{X}) = U(\mathbf{X}) = \frac{1}{2} \sum_{i=1}^{nb} E_i A_i \epsilon_i^2(\mathbf{X}) L_i(\mathbf{X}) \quad (17)$$

where  $\mathbf{X}$  is the vector of nodal coordinates, the subscript  $i \in \{1, \dots, nb\}$  indicates the bar index,  $E$  is the Young modulus of the material,  $A$  is the cross-sectional area,  $\epsilon$  is the axial strain, and  $L$  is the bar length. For a given  $\mathbf{X}$ , the strains  $\epsilon_i$  in Eq. (4) are the solutions of the elastic problem of the examined truss.

We start examining the BGA optimization of the simple truss in Figure 1, corresponding to a single control ( $N = 1$ ). In order to show the capability of the BGA to escape from the local minimum of the strain energy  $U$ , denoted  $a$  in Figures 2, 3, we executed the following three different runs: ES1 with population size  $\lambda = 12$ , mutation rate  $m = 0.20$ , and maximum number of generations  $g = 150$ ; ES2 with  $\lambda = 30$ ,  $m = 0.20$ , and  $g = 150$ ; and ES3 with  $\lambda = 12$ ,  $m = 0.20$ ,  $g = 250$ . In all the runs, we uploaded the configuration  $a$  in the initial generation (generation # 0) and let the vertical coordinate of the adaptive node to vary within the interval  $[0, 4]$ . We plot in Figure 4 the BGA evolutions obtained for each of the three examined cases, showing on the horizontal axis the generation number and on the vertical axis the corresponding best fitness. One can observe that the BGA quickly moves away from configuration  $a$ , even in the presence of a low mutation rate (runs ES2 and ES3), and converges to the global minimizer of the strain energy  $U$ , denoted  $c$  in Figures 2, 3. The fastest convergence rate was observed in the case with the largest population size (ES2).

The second example refers to the truss shown in Figure 5, where the *space of states* indicates the prescribed deformation

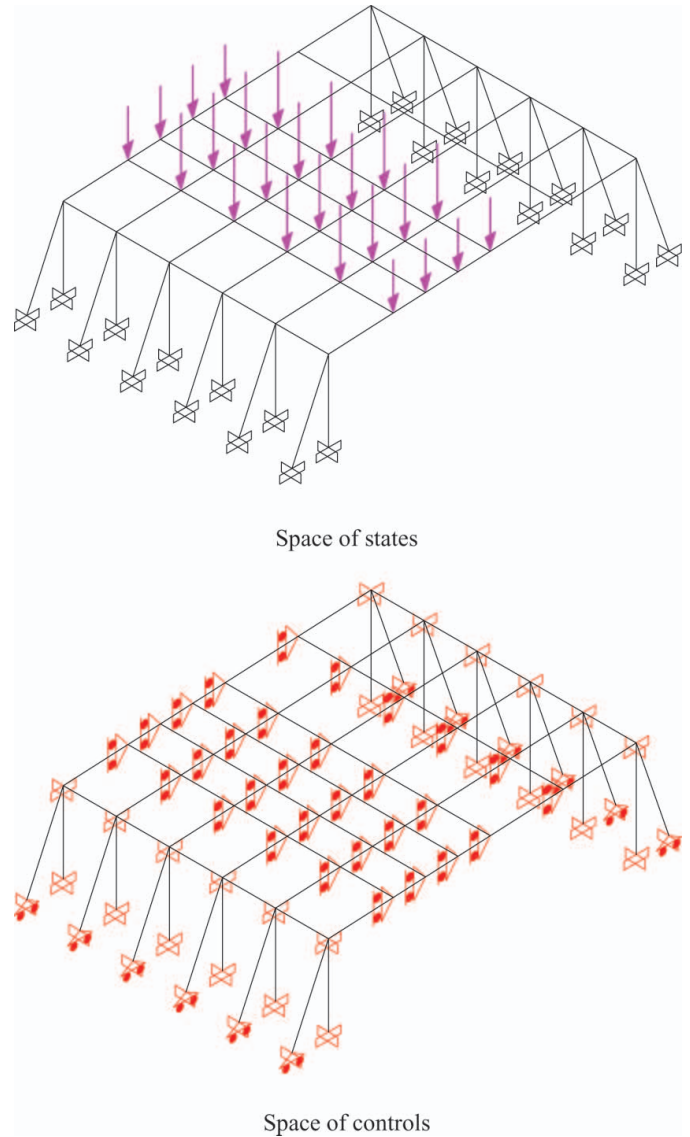


FIG. 9. Physical and design constraints for the optimal shape problem of a cable network (color figure provided online).

constraints and the *space of controls* indicates the design constraints, i.e., the limitations imposed on the controls. The nodes of the truss were constrained in a box of dimensions  $6L \times 4L$ , introducing a number of controls  $N = 9$  (cf. Figure 5, space of controls). All the bars are made of the same material and have equal cross-sectional area.

Figures 6–8 show the evolutions of the normalized best fitness  $J/FL$  and the optimal shape of the examined truss, for  $E = 2.48 \times 10^7 F/L^2$ , and  $A = 10^{-4} L^2$ . The optimal shape, shown in Figure 8, closely matches the one found by Braun in [70] where a gradient-based approach based on material forces was utilized.

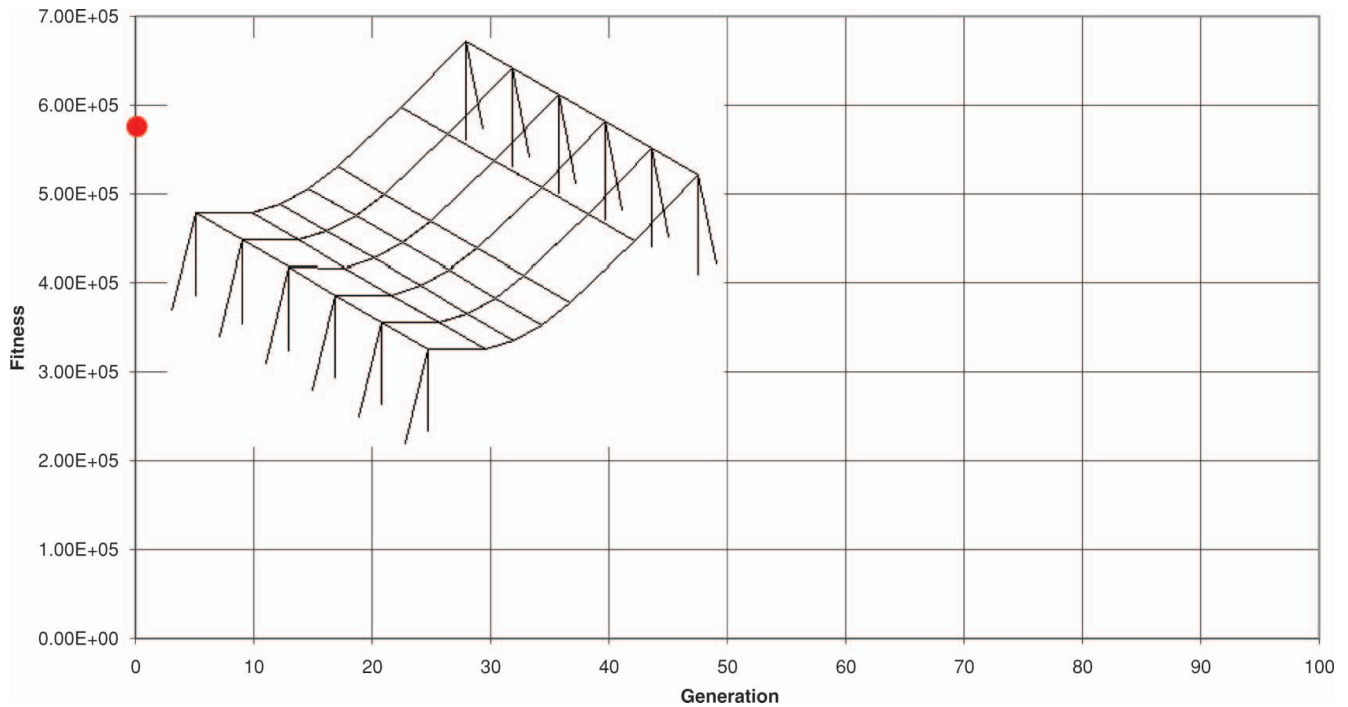


FIG. 10. BGA optimization of the structure in Figure 9: Best shape in correspondence with generation # 0. The horizontal axis shows the generation number and the vertical axis shows the corresponding best fitness  $J$  (daNcm). The best shape is shown within the plot.

#### 4.2. Funicular Curves as Minimum Compliance Shapes

In this section, we examine the possibility of determining the funicular curve of a given set of forces as the minimum compliance shape of a beam with small bending stiffness. We refer to the spatial structure in Figure 9, which is composed of six cables

constrained to vertical columns and to the ground. The cables carry four point loads of 1200 lb each spaced at 20 ft intervals, with the first load located at 40 ft from the closest column and the last one located at 90 ft from the opposite column. Due to this particular loading condition, the cables will remain in the

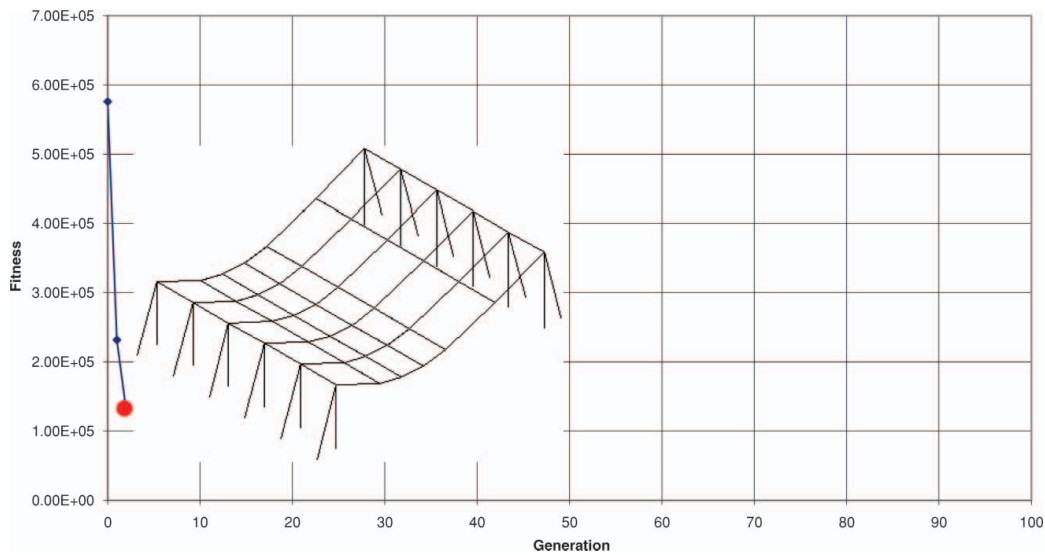


FIG. 11. BGA optimization of the structure in Figure 9: Best shape in correspondence with generation # 2. The horizontal axis shows the generation number and the vertical axis shows the corresponding best fitness  $J$  (daNcm). The best shape is shown within the plot.

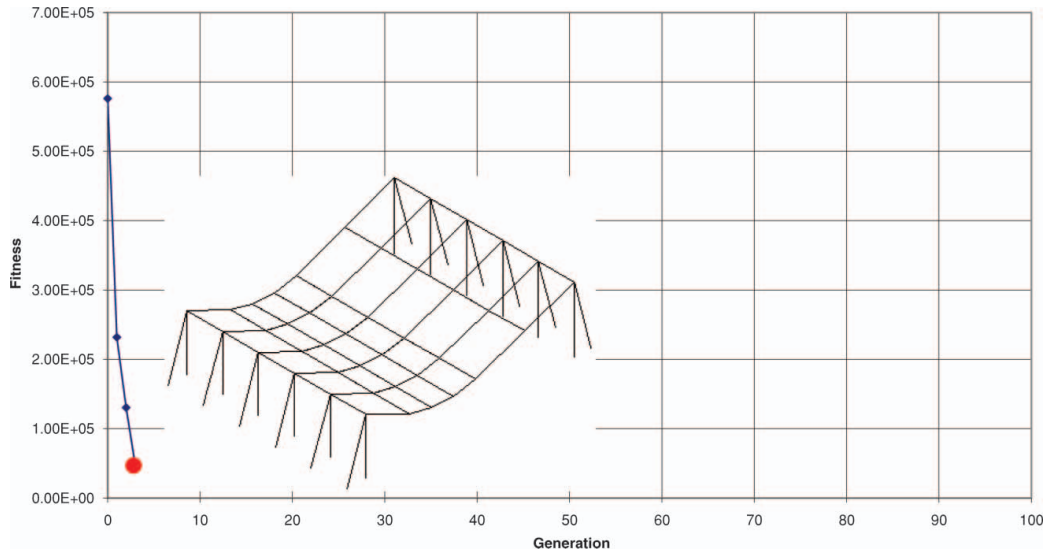


FIG. 12. BGA optimization of the structure in Figure 9: Best shape in correspondence with generation # 3. The horizontal axis shows the generation number and the vertical axis shows the corresponding best fitness  $J$  (daNcm). The best shape is shown within the plot.

planes containing the columns during deformation. The current example is extracted from Zalewski and Allen [3], where the optimal shape problem of a cable network supporting the ridge of an exhibition tent is studied through a graphical approach, constructing the funicular polygon through the columns, which gives a prescribed maximum force of 6600 lb in the cables (Figure 9, initial shape).

In the present model, the following strain energy fitness is introduced [69]:

$$J(\mathbf{X}) = U(\mathbf{X}) = \frac{1}{2} \sum_{i=1}^{nb} \int_{\Omega_i(\mathbf{X})} \left[ E_i A_i \epsilon_i^2(\mathbf{X}) + E_i I_i \theta_i^2(\mathbf{X}) \right] dx \tag{18}$$

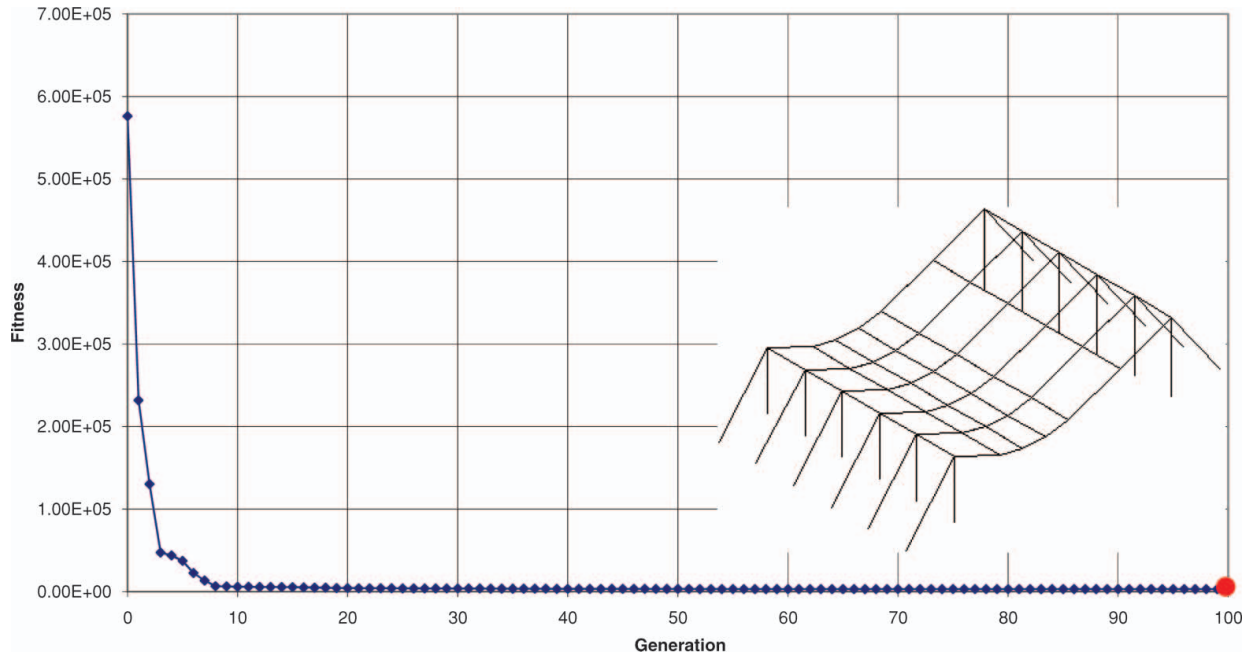


FIG. 13. BGA optimization of the structure in Figure 9: Best shape in correspondence with generation # 100. The horizontal axis shows the generation number and the vertical axis shows the corresponding best fitness  $J$  (daNcm). The best shape is shown within the plot.

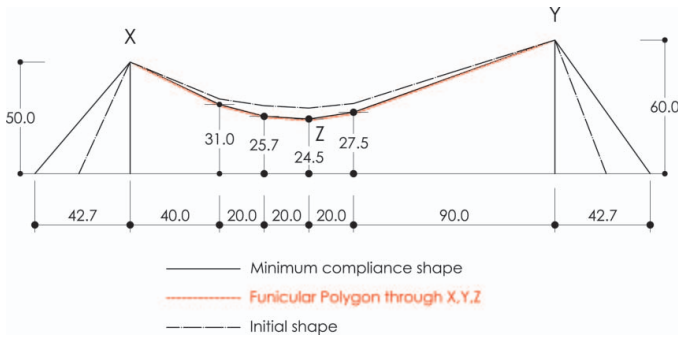


FIG. 14. Funicular polygon corresponding to the minimum compliance shape of the structure in Figure 9 (color figure provided online).

where  $i \in \{1, \dots, nb\}$  is the generic beam element id,  $\Omega(X)$  denotes the centerline, whose configuration depends on the control vector  $X$ ,  $\theta$  is the bending strain,  $I$  is the cross-sectional moment of inertia and  $x$  is a local coordinate. The generalized strains  $\epsilon_i$  and  $\theta_i$  in Eq. (18) are solutions of the elastic problem of the structure corresponding to a given  $X$ . For the sake of simplicity, we assume that the beams do not deform in shear (Bernoulli's theory), and refer to the following mechanical properties:  $E = 4.17 \times 10^9 \text{ lb/ft}^2$ ,  $A = 7.61 \times 10^{-3} \text{ ft}^2$ , and  $I = 10^{-6} \text{ ft}^4$  for the cables; and  $E = 4.17 \times 10^9 \text{ lb/ft}^2$ ,  $A = 4.01 \text{ ft}^2$  and  $I = 2.10 \times 10^5 \text{ ft}^4$  for the columns.

We performed an optimization of the shape given in [3] (*initial shape*), allowing the ground nodes of the cables to move horizontally in the space of controls, within 20 ft from the positions corresponding to such a shape. We also allowed the nodes in-between the columns to move vertically up to 6.5 ft with respect to the same shape. All the cables were forced to move in a self-similar way, introducing suitable master-slave constraints and a total of 7 controls (cf. Figure 9, space of controls). The evolution presented in Figures 10–13 shows that the BGA optimization converges in about 200 generations to a stable result (constant best fitness). Fig. 14 highlights that the BGA minimum compliance shape closely matches a funicular polygon through the columns. Indeed, due to the small bending stiffness of the cables, the strain energy minimization penalizes bending

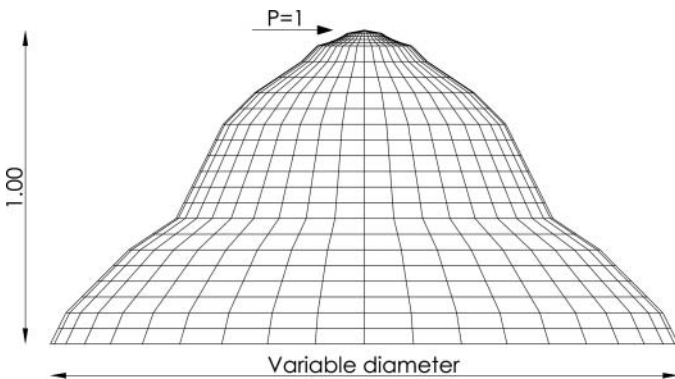


FIG. 15. Examined dome model.

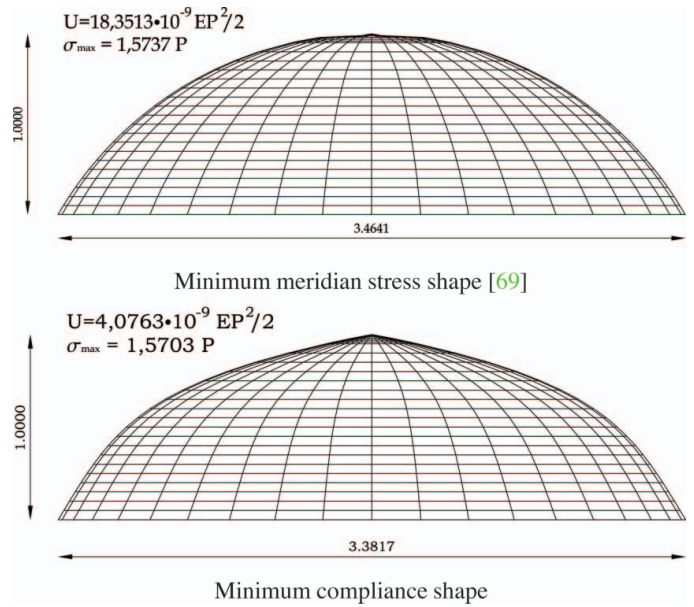


FIG. 16. Compliance optimization of a spherical dome.

deformation and leads the cables to assume a pure axial behavior. The minimum compliance funicular polygon corresponds to a 6305 lb maximum force in the cables.

### 4.3. Optimal Slopes of Roofs

In a recent article [71], Villaggio studied the best shapes of the meridians of a thin membrane of revolution loaded at

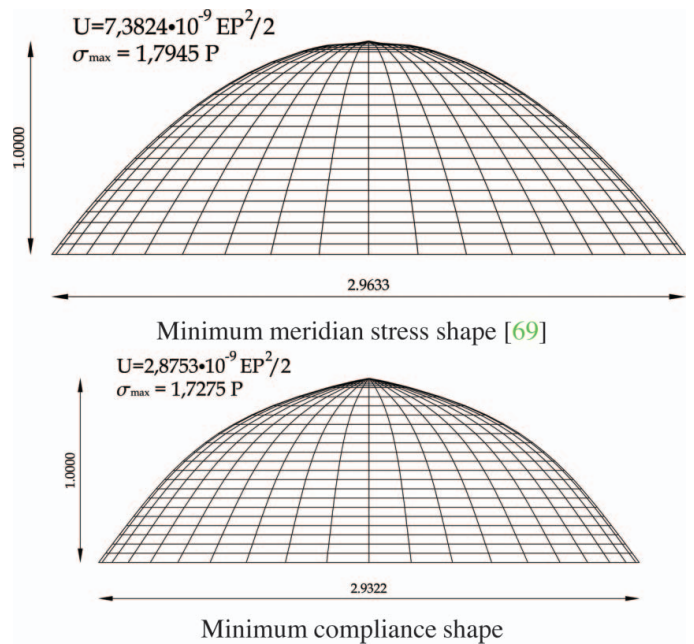


FIG. 17. Compliance optimization of a baroque dome.

the vertex by a horizontal force  $P$ , which is identified with the prototype of a roof structure (Figure 15). He considered several basic shapes (pyramidal, conical, spherical, parabolic, etc.) and optimized the size of the base diameter, keeping the shape fixed and the product thickness by the membrane surface area (material volume) constant. The objective function was let to coincide with the highest meridian stress at the basis of the membrane. Here, we deal with the search of local optima of three different reference shapes: spherical, “baroque” and “gothic”, following the notation of Villaggio. The latter two coincide with two special paraboloidal shells [71]. We uploaded in the first generation of the BGA evolution the best shape found by Villaggio (minimum meridian stress shape) for each of the three above cases, and let the 23 parallels of the finite element model in Figure 15 to deform, to some extent, with respect to the reference shape, conserving a polar-symmetric profile. We kept the material volume constant and equal to unity (as in [71]), by adjusting the membrane thickness. In order to perform a local optimization, we allowed the diameter  $d$  of each parallel to vary within the interval  $[(1 - 0.025) d^*, (1 + 0.025) d^*]$ ,  $d^*$  denoting the diameter corresponding to the reference shape (total number of controls:  $N = 23$ ). The finite element model was assumed to be in the pure elastic membrane regime, characterized by the

following strain energy fitness [69]

$$J(\mathbf{X}) = U(\mathbf{X}) = \frac{1}{2} \sum_{i=1}^{ns} \int_{\Omega_i(\mathbf{X})} \left\{ \frac{E_i h_i}{(1 - \nu^2)} \left[ (\epsilon_{i,1}(\mathbf{X}) + \epsilon_{i,2}(\mathbf{X}))^2 + 2(1 - \nu) \left( \frac{1}{4} \gamma_{i,12}^2(\mathbf{X}) - \epsilon_{i,1}(\mathbf{X}) \epsilon_{i,2}(\mathbf{X}) \right) \right] \right\} dx_1 dx_2 \quad (19)$$

Here,  $i \in \{1, \dots, nb\}$  is the generic shell element id,  $\Omega(\mathbf{X})$  denotes the shell middle surface, whose configuration depends on the control vector  $\mathbf{X}$ ,  $h$  is the membrane thickness,  $\epsilon_1, \epsilon_2$  and  $\gamma_{12}$  are in-plane extensional and shear strains, respectively, and  $x_1, x_2$  are local coordinates. It is understood that the generalized strains  $\epsilon_{i,1}, \epsilon_{i,2}$  and  $\gamma_{i,12}$  in (4.3) are solutions of the elastic problem of the examined finite element model for a given  $\mathbf{X}$ .

The minimum compliance shapes ( $\nu = 0.1$ ) are compared to the reference ones in Figures 16–18. Here,  $\sigma$  denotes the maximum meridian stress at the base of the dome. One can observe that the minimum compliance shapes do not conserve the same reference geometry (spherical or parabolic) and exhibit a remarkable lower compliance. In two cases (spherical and baroque domes), the minimum compliance shapes also exhibit smaller stress  $\sigma$ , while in the optimized gothic dome  $\sigma$  is slightly greater than in the case of the reference shape.

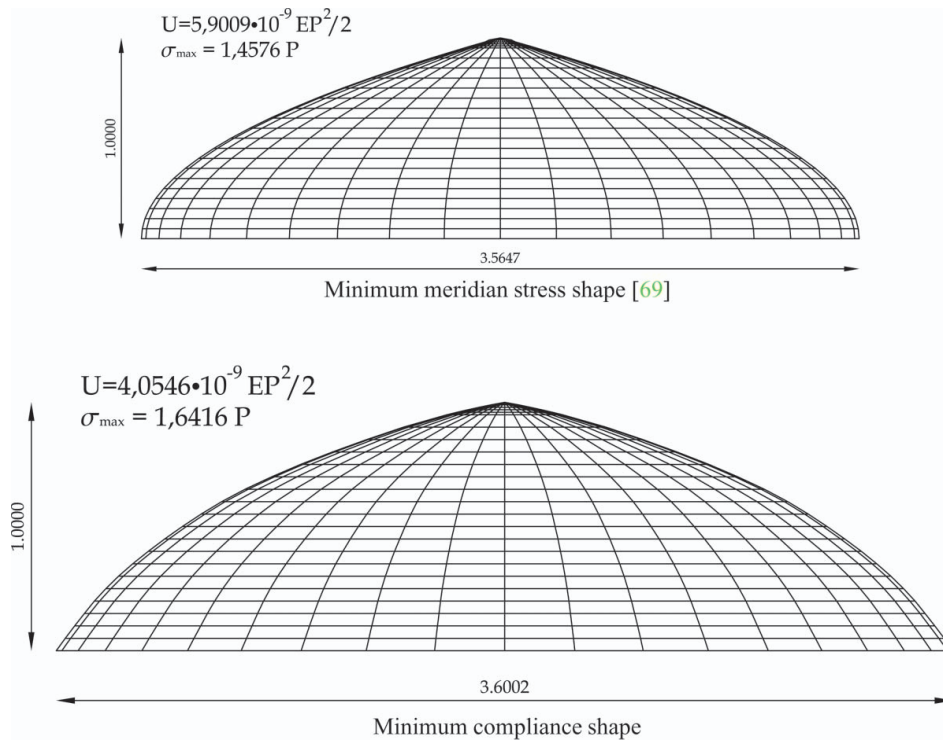
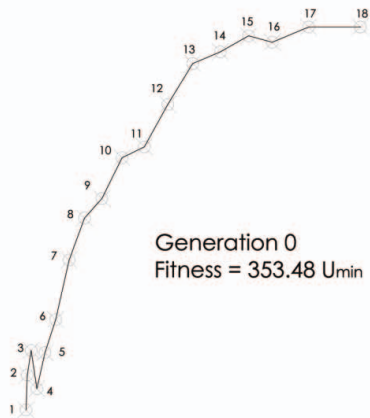
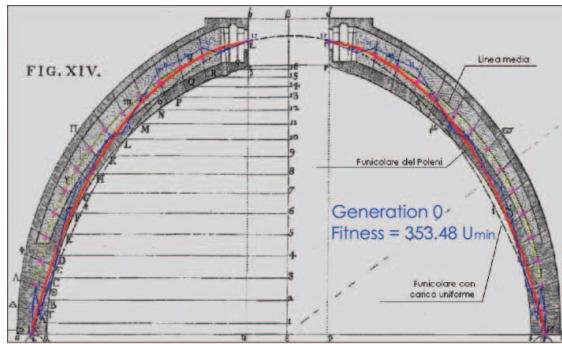
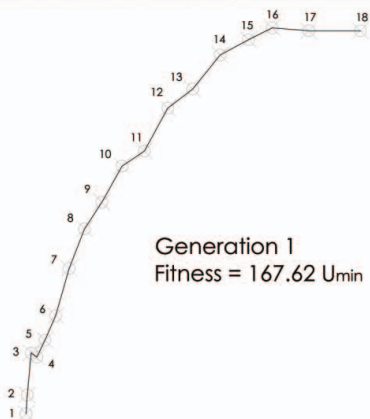
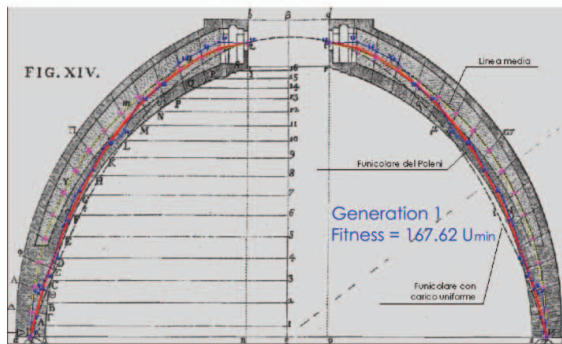


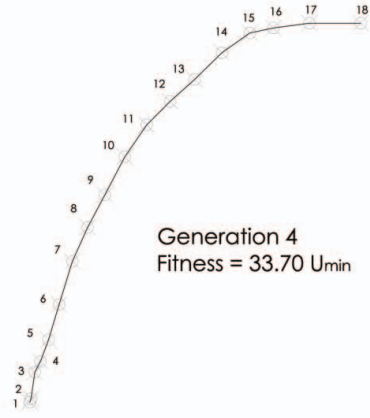
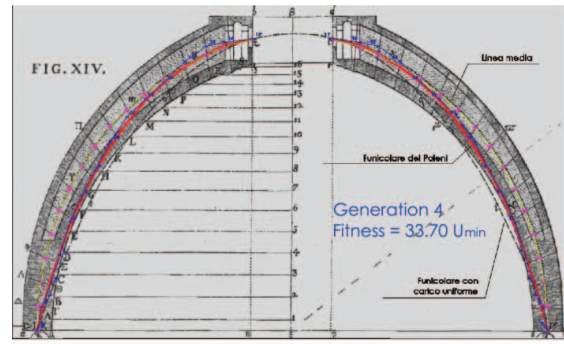
FIG. 18. Compliance optimization of a gothic dome.



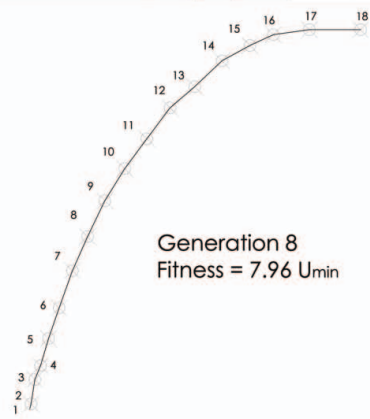
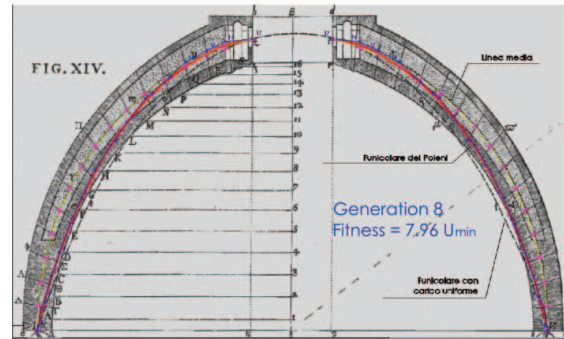
Generation # 0



Generation # 1



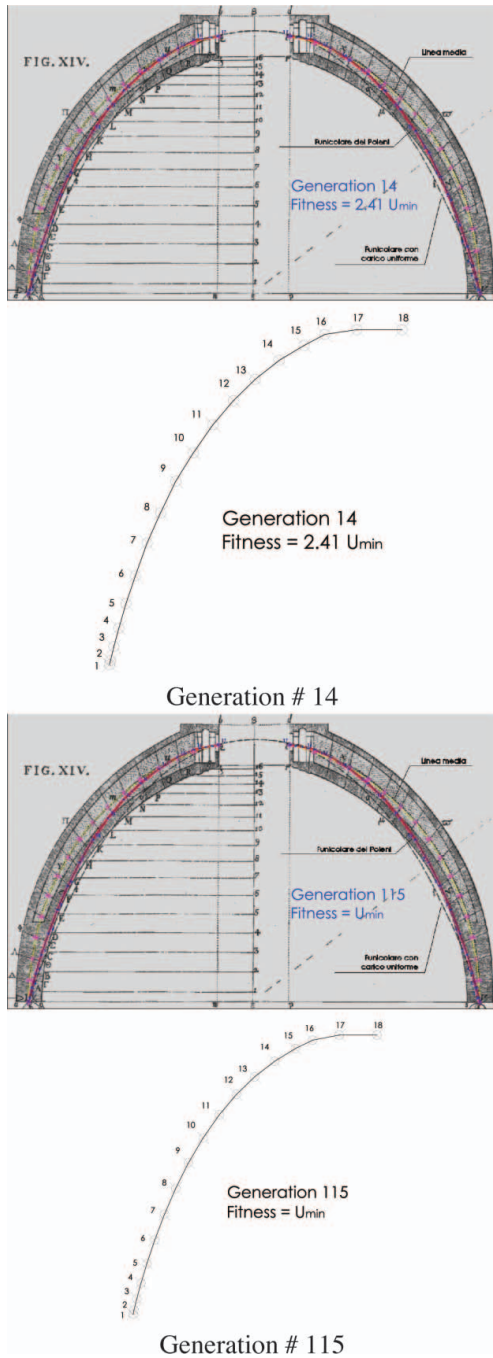
Generation #4



Generation # 8

FIG. 19. (Color online, adapted from [56]) BGA evolution of the funicular profile of St. Peter's cupola: Generations 0 and 1 (red/light solid line: Poleni's funicular polygon; dark/marked solid line: current best BGA shape) (color figure provided online).

FIG. 20. (Color online, adapted from [56]) BGA evolution of the funicular profile of St. Peter's cupola: Generations 4 and 8 (red/light solid line: Poleni's funicular polygon; dark/marked solid line: current best BGA shape) (color figure provided online).



#### 4.4. On the Optimal Shape of St. Peter's Cupola in Rome

St. Peter's cupola in Vatican, Rome, was completed in 1588 under the direction of Giacomo della Porta, who slightly changed a previous design by Michelangelo Buonarroti, developed in the period 1548–1561 [57]. Della Porta raised Michelangelo's profile, taking the height of the structure to 136 meters. A

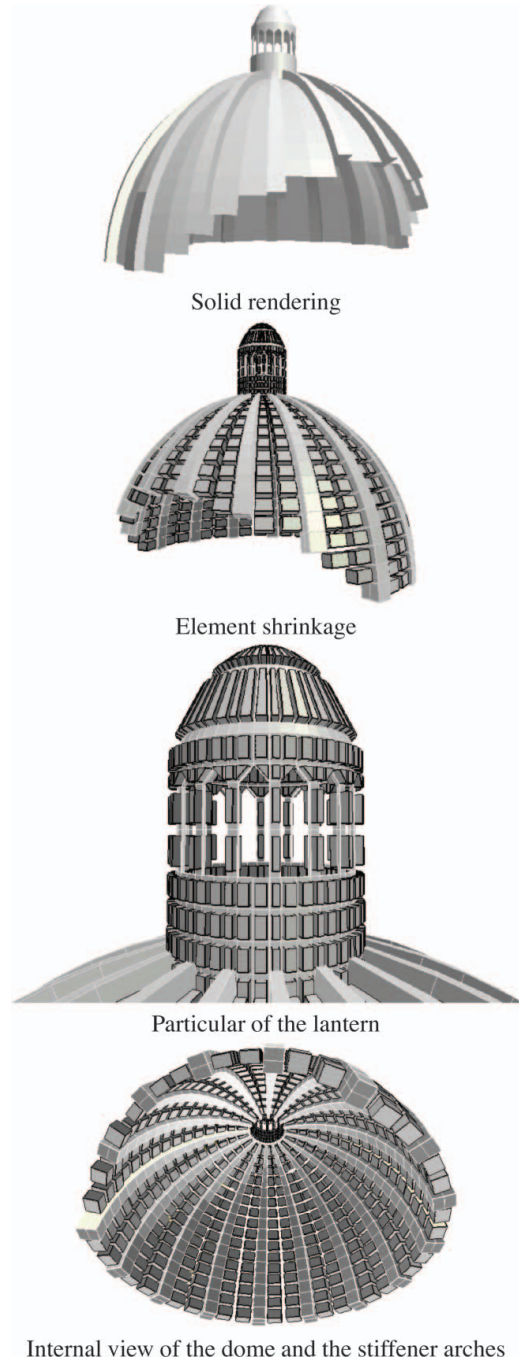


FIG. 22. 3D finite element model of St. Peter's cupola (1237 shell elements and 1297 nodes).

central point of the study of Giovanni Poleni [56] on the statics of St. Peter's cupola consisted of the determination of the funicular curve of the self-weight loading. Poleni examined a meridian slice of the cupola, corresponding to 1/50 of the full structure, and divided each of the two symmetric halves (separated by the central lantern) into 17 parts (cf. Figure 19). He accurately computed the self weight of each of those parts (partially hollow, due

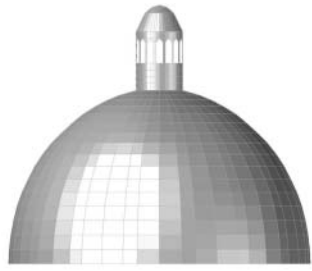
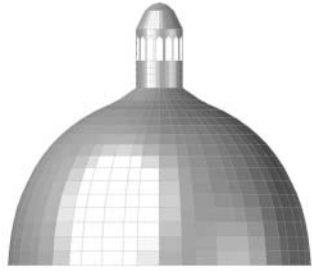
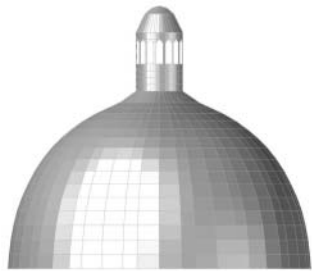
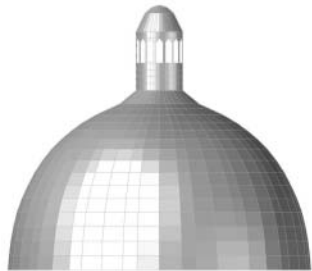
Generation 0 ( $U = 1.911 U_{min}$ )Generation 10 ( $U = 1.566 U_{min}$ )Generation 15 ( $U = 1.505 U_{min}$ )Generation 20 ( $U = 1.501 U_{min}$ )

FIG. 23. BGA evolution of a 3D finite element model of St. Peter's cupola: Generations 0, 10, 15 and 20.

to the presence of internal stairs) and applied a force proportional to their weights to vertical lines containing the corresponding centers of mass. Finally, he constructed the funicular polygon of this system of vertical forces, which passes through the center of the base section and mid-sections (Figure 19, red/light solid line). The no-tension constitutive model for masonry structures

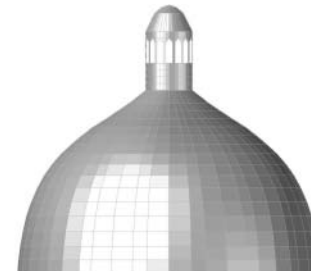
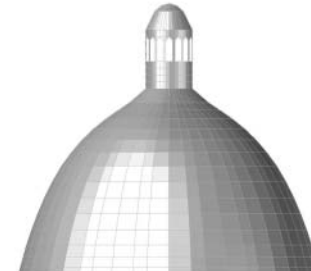
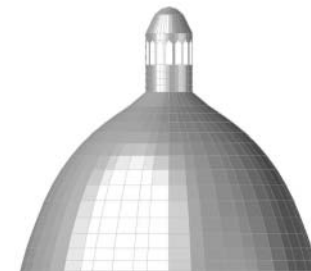
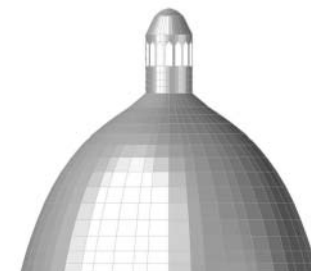
Generation 25 ( $U = 1.444 U_{min}$ )Generation 100 ( $U = 1.030 U_{min}$ )Generation 150 ( $U = 1.029 U_{min}$ )Generation 250 ( $U = 1.016 U_{min}$ )

FIG. 24. BGA evolution of a 3D finite element model of St. Peter's cupola: Generations 25, 100, 150 and 250.

(like the cupola) assumes that the modeled material does not react at all in tension, and demands that the funicular polygon entirely lies within the thickness of the dome in order to ensure structural stability (cf., e.g., Heyman [1]). One can observe that Poleni's funicular polygon is approximately tangent to the intrados of the cupola in correspondence with the zones located at

TABLE 1

Mean surface area ( $\text{mm}^2$ ) and volume ( $\text{mm}^3$ ) of the BGA best shapes of St. Peter's cupola for different generations.

Gen.	Surface	Volume
0	$0.32373968E + 10$	$0.65380674E + 13$
100	$0.32331894E + 10$	$0.65318783E + 13$
150	$0.32344964E + 10$	$0.65341877E + 13$
200	$0.32394134E + 10$	$0.65430633E + 13$
250	$0.32527797E + 10$	$0.65792475E + 13$
1085	$0.30765911E + 10$	$0.59453908E + 13$
1634	$0.30766364E + 10$	$0.59437801E + 13$
2367	$0.30668530E + 10$	$0.59119369E + 13$
3499	$0.30467765E + 10$	$0.58462119E + 13$

1/4 of the span from the impost (Figure 19). This indicates the presence of high compressive stresses at the intrados and possible fracture damage at the extrados in these areas, which were indeed affected by diffuse cracking at the time of Poleni's study. Poleni and Luigi Vanvitelli, another architect consulted by Pope Benedict XIV, suggested to restore the cupola by applying large iron rings to be bolted to the dome. This retrofit intervention was successfully carried out in 1748.

Proceeding as in section 4.2. we numerically computed Poleni's funicular arch as the minimum compliance shape of a beam with small bending stiffness. We considered a collection of 17 beams, corresponding to the different elements of the cupola's slice analyzed by Poleni. The cross-sectional areas of these elements vary between  $1.27 \times 10^6 \text{ mm}^2$  and  $5.27 \times 10^6 \text{ mm}^2$ . An axial to bending thickness ratio equal to 50 was introduced to penalize bending deformation. The nodes from 2 to 16 (Figure 19) of the beam collection were allowed to move vertically within the intrados and the extrados of the cupola ( $N = 15$ ). Equation (18) was employed for the model fitness. Figures 19–21 show that the BGA minimum compliance shape converges to Poleni's funicular polygon in about 115 generations. The fitness (strain energy) of the first best shape (generation # 0) is approximately 350 times larger of that corresponding to the final one (generation # 115).

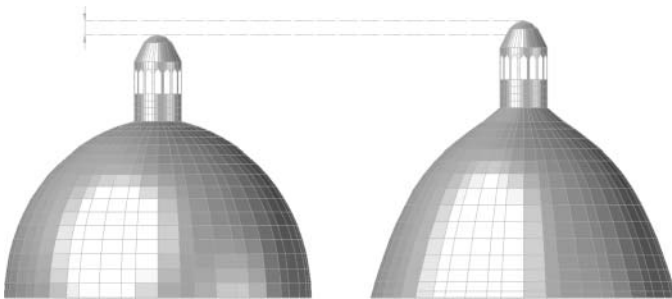


FIG. 25. Comparison between the actual shape (left,  $U = 1.911 U_{min}$  Nmm) and the virtual minimum compliance shape (right,  $U = U_{min}$ , generation # 300) of St. Peter's cupola.

We subsequently carried out a 3D analysis of the cupola, employing a finite element model made up of variable thickness shell elements in the pure membrane regime ( $h_{max} = 2839 \text{ mm}$ ,  $h_{min} = 25 \text{ mm}$ ). The model was reconstructed from the structural details of the cupola given in [56], and includes dome elements, stiffener arches and the lantern (Figure 22).

A (virtual) compliance optimization of the 3D (real) cupola model was carried out by letting the shell nodes to move within the intrados and the extrados of the real cupola. Equation (19) was employed as a fitness measure. In contrast to the 2D model, the base nodes in the 3D case were allowed to move in the horizontal plane and the vertex nodes were allowed to move in the vertical direction, always within the thickness of the real cupola. Polar symmetry was preserved introducing a unique control variable for each parallel of the model with a total of  $N = 18$  controls. The thickness of the shell elements was kept constant and coincident with that of the real cupola, and the latter was uploaded as a particular individual in generation # 0. The minimum compliance shapes corresponding to different BGA generations (for  $E = 19, 600 \text{ N/mm}^2$  and  $\nu = 0.1$ ) are shown in Figures 23, 24. Convergence to a stable shape was observed in about 3500 generations. Table 1 shows the corresponding evolution of the cupola mean surface area and volume. One can observe that the minimum compliance shape of the cupola, compared to the actual shape, is slightly slenderer, and has a strain energy  $U$  about 20 times smaller (Figure 25). In particular, the base diameter of the optimal shape is 0.2 m smaller than that of the real one, and its rise is about 2 m taller. Poleni [56], in his treatise, concluded that the fracture damage observed at that time in the cupola was mainly due to its insufficient rise and that a slightly more slender shape would have ensured a safer structural behavior. It is interesting to note that we are led to a quite similar result through a purely numerical approach. It is worthwhile noting that the original profile of the cupola designed by Michelangelo Buonarrotti was even shorter than the more "baroque" shape created by Giacomo della Porta in 1588. It is indeed an accepted opinion that the more "circular" shape of Michelangelo's would have induced stability problems in the cupola, as it is argued, e.g., in a recent study by Federico Bellini [57].

## 5. CONCLUDING REMARKS

We have presented a variational formulation of ground-structure approaches to structural optimization within the framework of optimal control problems [53]. Existence of solutions has been proved in general form, for arbitrary ground structures, referring to the case of geometry optimization of discrete models and minimum compliance problems. Non-uniqueness of the solution, for the same problems, has been shown by way of example.

A numerical procedure for shape (geometry) optimization of discrete models has also been presented, based on a Breeder Genetic Algorithm [48] belonging to the family of Evolutionary Algorithms. Numerical applications have shown that the pre-

sented procedure is well suited for shape optimization of discrete structural models, being able to escape from local minima of the fitness function. Moreover, the presented numerical implementations offer classical tools of shaping structures, such as graphical constructions of funicular curves and optimal thrust surfaces, and can be thought of as an automatic approach to the first phase of the conceptual design of a structure, dealing with simple bounds on the design variables. The presented results examine the optimal shape of trusses, beams and domes. A specific application has been dedicated to the study of the optimal shape of St. Peter's cupola in Rome, confirming the well documented conclusions of the treatise by Giovanni Poleni [56]. Rather fast convergence of the algorithm to the optimal shape was recorded in each of the examined examples. An excellent agreement between the presented approach and other optimization methods available in the literature has been observed.

The given optimization strategy requires little knowledge of the search environment, can be usefully interfaced with standard software packages of structural analysis, and can be easily generalized to nonlinear and/or dynamical optimization problems. Further generalizations may regard inclusion of general constraints, multi-objective and multi-functional optimization of structures, integrating architectural, structural and mechanical performance criteria, and conceptual design of complex structural shapes [46]. Also, the presented methods can be used to obtain optimal shapes of innovative membranes and domes, as well as optimal tensegrity and depolyable structures. Furthermore, it is particularly interesting to emphasize the conjunct use of evolutionary strategies and the lumped stress method recently proposed in [72–74], for the analysis of continuous shape optimization problems through consistent discrete approximations.

## ACKNOWLEDGMENTS

The authors would like to thank Fabio Formato, graduate student at the Department of Civil Engineering of the University of Salerno, for his precious collaboration with the numerical study on the optimal shape of St. Peter's cupola. F.F. greatly acknowledges the support of the Italian MIUR through the 2007 grant "Energetic Methods in Fracture Mechanics and Biomechanics."

## REFERENCES

- J. Heyman, *The Stone Skeleton*. Cambridge University Press, New York, 1995.
- E. Benvenuto, *La Scienza delle Costruzioni ed il suo Sviluppo Storico*. Manuali Sansoni, Firenze, 1981.
- W. Zalewski and E. Allen, *Shaping Structures: Statics*. John Wiley & Sons, New York, 1998.
- B. Kraft. Conceptual Design Tools for Civil Engineering. In M. Nagl J.L. Pfaltz and B. Böhlen, editors, *Applications of Graph Transformations with Industrial Relevance*, pp. 434–439. Springer Berlin, Heidelberg, 2003. AGTIVE 2003, Charlottesville, VA, USA.
- J. Szuba, A. Ozimek, and A. Schürr. On Graphs in Conceptual Engineering Design. In M. Nagl J.L. Pfaltz and B. Böhlen, editors, *Applications of Graph Transformations with Industrial Relevance*, pp. 75–89. Springer Berlin, Heidelberg, 2003. AGTIVE 2003, Charlottesville, VA, USA.
- M.I. Jimenez Morales, Gaudi, *La Búsqueda de La Forma: Espacio, Geometría, Estructura y Construcción*. Lunwerg Editores, Barcelona, 2002.
- A.G.M. Michell. The Limits of Economy of Materials in Frame Structures, *Philos. Mag.*, Series 6, vol. 8, no., 47, pp. 589–597, 1904.
- W.C. Dorn, R.E. Gomory, and H.J. Greenberg. Automatic Design of Optimal Structures, *J. Mecanique*, vol. 3, pp. 25–52, 1964.
- U.T. Ringertz. On Topology Optimization of Trusses, *Eng. Optimiz.*, vol. 9, pp. 209–218, 1985.
- M. Ohsaki. Simultaneous Optimization of Topology and Geometry of a Regular Plane Truss, *Comput. Struct.*, vol. 66, no., 1, 69–77, 1998.
- G.I.N. Rozvany and M. Zou. Layout and Generalized Shape Optimization by Iterative coc Method. In G. I. N. Rozvany, editor, *Optimization of Large Structural Systems*, vol. 1, pp. 103–120. Kluwer Academic Publishers, Dordrecht, 1993. NATO/DFG ASI.
- P. Pedersen. Topology Optimization of Three Dimensional Trusses. In C. A. Mota Soares M. P. Bendsøe, editor, *Topology Design of Structures*, vol. 227, pp. 19–30. Kluwer Academic Publishers, Dordrecht, 1990. NATO ASI Series E: Applied Sciences.
- M.P. Bendsøe. *Optimization of Structural Topology, Shape and Material*. Springer, Berlin, Heidelberg, New York, 1995.
- G.I.N. Rozvany and T. Birker. Generalized Michell structures – Exact Least-weight Truss Layouts for Combined Stress and Displacements Constraints. Part I: General Theory for Plane Trusses, *Struct. Optimization*, vol. 9, pp. 78–86, 1995.
- U. Kirsch. Integration of Reduction and Expansion Processes in Layout Optimization, *Struct. Optimization*, vol. 11, pp. 13–18, 1996.
- M. Zhou. Difficulties in Truss Topology Optimization with Stress and Local Buckling Constraints, *Struct. Optimization*, vol. 11, pp. 134–136, 1996.
- M.P. Bendsøe and N. Kikuchi. Generating Optimal Topologies in Structural Design using a Homogenization Method, *Comput. Methods Appl. Mech. Eng.*, vol. 71, pp. 197–224, 1988.
- M.P. Bendsøe. Optimal Shape as a Material Distribution Problem, *Struct. Optimization*, vol. 1, pp.193–202, 1989.
- M.P. Bendsøe, J. Rasmussen, and H.C. Rodriguez. Topology and Boundary Shape Optimization as an Integrated Tool for Computer Aided Design. In *Lecture Notes in Engineering*, vol. 63, pp. 27–34. Springer-Verlag, Berlin, 1990.
- N. Kikuchi, K. Suzuki, and J. Fukushima. Layout Optimization using the Homogenization Method: Generalized Layout Design of Three-dimensional Shells for Car Bodies. In G. I. N. Rozvany, editor, *Optimization of Large Structural System*, vol. 3, pp. 110–126. Berchtesgaden, 1991. NATO-ASI Series.
- M.P. Bendsøe, A.R. Diaz, and J.E. Taylor. On the Prediction of Extremal Material Properties and Optimal Material Distribution for Multiple Loading Condition. In 20th Design Automation Conference American Society of Mechanical Engineers, vol. 69–2, pp. 213–220. ASME, New York, 1994.
- Z.D. Ma, N. Kikuchi, H.C. Cheng, and I. Hagiwara. Topological Optimization Technique for Free Vibration Problems, *J. Appl. Mech-T. ASME*, vol. 62, pp. 200–207, 1995.
- J.B. Jacobsen, N. Olhoff, and E. Rønholt. Generalized Shape Optimization of Three-dimensional Structures using Materials with Optimum Microstructures, *Mech. Mater.*, vol. 28, pp. 207–225, 1998.
- A.H.G. Allaire. On Some Recent Advances in Shape Optimization, volume 329. C. R. Acad. Sci., Paris, 2001.
- S. Schwarz, K. Maute, and E. Ramm. Topology and Shape Optimization for Elastoplastic Structural Response. *Comput. Methods Appl. Mech. Eng.*, vol. 190, pp. 2135–2155, 2001.
- M.P. Bendsøe and O. Sigmund. *Topology Optimization: Theory, Methods and Applications*. Springer Verlag, Berlin Heidelberg, 2003.
- R. Kemmer, A. Lipka, and E. Ramm. Large Deformations and Stability in Topology Optimization, *Struct. Multidiscip. O.*, vol. 30, pp. 459–476, 2005.
- M. Save and W. Prager (eds.). *Structural Optimization, Optimality Criteria*. Plenum Press, New York, 1985.

29. L. Berke and N.S. Knot. Structural Optimization using Optimality Criteria. In C. A. Mota Soares, editor, *Computer Aided Optimal System: Structural and Mechanical Systems*, pp. 271–311. Springer-Verlag, Berlin, 1987.
30. C. Fleury and V. Braibant. Structural Optimization: A New Dual Method using Mixed Variables, *Int. J. Numer. Meth. Eng.*, vol. 23, pp. 409–428, 1986.
31. K. Svanberg. The Method of Moving Asymptotes: A New Method for Structural Optimization, *Int. J. Numer. Meth. Eng.*, vol. 24, pp. 359–373, 1987.
32. C. Fleury. Efficient Approximation Concepts using Second Order Information, *Int. J. Numer. Meth. Eng.*, vol. 28, pp. 2041–2058, 1987.
33. Z.D. Ma and N. Kikuchi. A New Method of the Sequential Approximate Optimization, *Eng. Optimiz.*, vol. 25, pp. 231–253, 1995.
34. Y.M. Xie and G.P. Steven. A Simple Evolutionary Procedure for Structural Optimization, *Comput. Struct.*, vol. 49, pp. 885–896, 1993.
35. Y. M. Xie and G. P. Steven. *Evolutionary Structural Optimization*. Springer, London, 1997.
36. P. Tanskanen. A Multiobjective and Fixed Elements Based Modification of the Evolutionary Structural Optimization Method, *Comput. Methods Appl. Mech. Eng.*, vol. 196, pp. 76–90, 2006.
37. R.J. Balling. Optimal Steel Frame Design by Simulated Annealing, *J. Struct. Eng.-ASCE*, vol. 117, 1991.
38. P.Y. Shim and S. Manoochemri. Generating Optimal Configurations in Structural Design using Simulated Annealing, *Int. J. Numer. Meth. Eng.*, vol. 40, pp. 1053–1069, 1997.
39. D.E. Golberg and M.P. Samtani. Engineering Optimization via Genetic Algorithm, *Proc., 9th Conf. Electronic Computation, ASCE*, pp. 471–482, 1986.
40. W.M. Jenkins. Plane Frame Optimum Design Environment Based on Genetic Algorithm, *J. Struct. Eng.-ASCE*, vol. 118, 1992.
41. P. Hajela, E. Lee, and C.Y. Lin. Genetic Algorithms in Structural Topology Optimization. In C. A. Mota Soares M. P. Bendsøe, editor, *Topology Design of Structures*, vol. 227, pp. 117–133. Kluwer Academic Publishers, Dordrecht, 1990. NATO ASI Series E: Applied Sciences.
42. C.D. Chapman, K. Saitou, and M.J. Jakiela. Genetic Algorithms as an Approach to Configuration and Topology Design, *J. Mech. Design*, vol. 116, pp. 1005–1012, 1994.
43. S.D. Rajan. Sizing, Shape and Topology Design Optimization of Trusses using Genetic Algorithm, *J. Struct. Eng.-ASCE*, vol. 121, no. 10, pp. 1480–1487, 1995.
44. I. De Falco, R. Del Balio, A. Della Cioppa, and E. Tarantino. A Comparative Analysis of Evolutionary Algorithms for Function Optimisation. In *Proceedings of the Second Workshop on Evolutionary Computation (WEC2)*, pp. 29–32. Nagoya, JAPAN, 1996.
45. G. Steven, O. Querin, and M. Xie. Evolutionary Structural Optimisation (eso) for Combined Topology and Size Optimisation of Discrete Structures, *Comput. Methods Appl. Mech. Eng.*, vol. 188, pp. 743–754, 2000.
46. R. Kicinger, T. Arciszewsky, and K. De Jong. Evolutionary Computation and Structural Design: A Survey of the State-of-the-art, *Computers and Structures*, vol. 83, no. 23–24, pp. 1943–1978, 2006.
47. H. Mühlenbein and D. Schlierkamp-Voosen. The Science of Breeding and its Application to the Breeder Genetic Algorithm (BGA), *Evol. Comput.*, vol. 1, no. 4, pp. 335–360, 1994.
48. I De Falco, R. Del Balio, A. Della Cioppa, and E. Tarantino. Optimising Constrained Continuous Multivariable Functions with Breeder Genetic Algorithms, *Journal of Evolutionary Optimization*, vol. 1, no. 1, pp. 53–64, 1999.
49. C. Mattheck and S. Burkhardt. A New Method of Structural Shape Optimization based on Biological Growth, *Int. J. Fatigue*, vol. 12, no. 3, pp. 185–190, 1990.
50. Z. Mróz and D. Bojczuk. Topological Derivative and its Application in Optimal Design of Truss and Beam Structures for Displacement, Stress and Buckling Constraints. In G. I. N. Rozvany, editor, *Topology Optimization of Structures and Composite Continua*, pp. 91–105. Kluwer, Dordrecht, Boston, London, 2000.
51. Z. Mróz and D. Bojczuk. Finite Topology Variations in Optimal Design of Structures, *Struct. Multidiscip. O.*, vol. 25, pp. 153–173, 2003.
52. R.V. Kohn. Optimal Design and Relaxation of Variational Problems, *Comm. Pure Appl. Math.*, vol. 36, pp. 113–137, 1986.
53. D. Bucur and G. Buttazzo. Variational Methods in Shape Optimization Problems. In *Progress in Nonlinear Differential Equations and Their Applications*, volume 65. Birkhauser, Boston, 2005.
54. S. Pezeshk. State of the Art on the use of Genetic Algorithms in Design of Steel Structures. In S. Burns, editor, *Recent Advances in Optimal Structural Design*. Reston, VA, 2002.
55. I De Falco, R. Del Balio, A. Della Cioppa, and E. Tarantino. Evolutionary Algorithms for Aerofoil Design, *Int. J. Comput. Fluid D.*, vol. 11, no. 1, pp. 51–77, 1998.
56. G. Poleni. *Memorie storiche della gran cupola del Tempio Vaticano*. Edizioni Kappa, Rome, Italy, 1991. (*Anastatic reprint of the original edition of 1748*).
57. F. Bellini. *La cupola di San Pietro da Michelangelo a Della Porta*. Nuova Argos, Rome, Italy, 2011.
58. P. Thoutireddy and M. Ortiz. A Variational R-adaption and Shape Optimization Method for Finite Deformation Elasticity, *Int. J. Numer. Meth. Eng.*, vol. 61, pp. 1–21, 2004.
59. J. Mosler and M. Ortiz. On the Numerical Implementation of Variational Arbitrary Lagrangian-Eulerian (VALE) formulations, *Int. J. Numer. Meth. Eng.*, vol. 67, pp. 1272–1289, 2006.
60. J.E. Marsden and A. Weinstein. *Calculus*. Springer, New York, NY, 1985.
61. M. Ortiz and A. Stainer. The Variational Formulation of Viscoplastic Constitutive Updates. *Comput. Method Appl. Mech. Eng.*, vol. 171, pp. 419–444, 1999.
62. G. Dal Maso, G.A. Francfort, and R. Toader. Quasistatic Crack Growth in Nonlinear Elasticity, *Arch. Rational Mech. Anal.*, vol. 176, no. 2, pp. 165–225, 2005.
63. G. Dal Maso, A. De Simone, and M.G. Mora. Quasistatic Evolution Problems for Linearly Elastic - perfectly Plastic Materials, *Arch. Rational Mech. Anal.*, vol. 180, pp. 237–291, 2006.
64. G. Dal Maso, A. De Simone, M.G. Mora, and M. Morini. A Vanishing Viscosity Approach to Quasistatic Evolution in Plasticity with Softening, *Preprint SISSA*, 38/2006/M:1–58, 2006.
65. A. Mielke and M. Ortiz. A Class of Minimum Principles for Characterizing the Trajectories and the Relaxation of Dissipative Systems, *ESAIM COCV*, in press.
66. F. Fraternali, M.A. Porter, and C. Daraio. Optimal Design of Granular Protectors (preprint), *Division of Engineering and Applied Science, California Institute of Technology*, 2008.
67. K.A. De Jong. *Evolutionary Computation. A Unified Approach*. MIT Press, 2006.
68. Sap2000<sup>©</sup>. *Linear and Nonlinear Static and Dynamic Analysis and Design of Three-dimensional Structures. Basic Analysis Reference Manual*. Computers and Structures, Inc., Berkeley, CA, 2006. Version 11.
69. K. Washizu. *Variational Methods in Elasticity and Plasticity*. Pergamon Press, Oxford, UK, 1975. 2nd Edition.
70. M. Braun. Structural Optimization by Material Forces. In P. Steinmann and G.A. Maugin, editors, *Advances in Mechanics and Mathematics*, volume 11: *Mechanics of Material Forces*, pp. 211–218. Springer US, 2005.
71. P. Villaggio. The slope of roofs, *Meccanica*, vol. 35, pp. 215–227, 2000.
72. F. Fraternali. Complementary Energy Variational Approach for Plane Elastic Problems with Singularities, *Theor. Appl. Fract. Mech.*, vol. 35, pp. 129–135, 2001.
73. F. Fraternali. Error Estimates for a Lumped Stress Method for Plane Elastic Problems, *Mech. Adv. Mat. Struct.*, vol. 14, pp. 309–320, 2007.
74. F. Fraternali, A. Angelillo, and F. Fortunato. A Lumped Stress Method for Plane Elastic Problems and the Discrete-continuum Approximation, *Int. J. Solids Struct.*, vol. 39, pp. 6211–6240, 2002.